CO 2 electroreduction in water with a heterogenized Csubstituted Nickel cyclam catalyst

Silvia Pugliese, Ngoc Tran Huan, Albert Solé-Daura, Yun Li, Jose-Guillermo Rivera de la Cruz, Jérémy Forte, Sandrine Zanna, Alain Krief, Bao-Lian Su, Marc Fontecave

CO_2 electroreduction in water with a heterogenized C-substituted Nickel cyclam catalyst

*Silvia Pugliese,[1,2] Ngoc Tran Huan,[1] Albert Solé-Daura,[1] Yun Li,[1] Jose-Guillermo Rivera de la Cruz,[1] Jérémy Forte,[3] Sandrine Zanna,[4] Alain Krief,[2] Bao-Lian Su,[2] Marc Fontecave[1]**

1. Laboratoire de Chimie des Processus Biologiques, UMR CNRS 8229, Collège de France-CNRS-Sorbonne Université, PSL Research University,11 Place Marcelin Berthelot, 75231 Paris Cedex 05, France.

2. Laboratory of Inorganic Materials Chemistry (CMI), University of Namur, 61 rue de Bruxelles, B-5000 Namur, Belgium

3. Institut Parisien de Chimie Moléculaire, UMR 8232 CNRS, Plateforme DRX, Sorbonne Université, 4 place Jussieu, 75252 Paris Cedex 5, France

4. PSL Research University - CNRS Institut de Recherche de Chimie Paris (IRCP), 11 rue Pierre et Marie Curie, 75005 Paris, France

*Corresponding author. Email: marc.fontecave@college-de-france.fr

Keywords: CO_2 electroreduction, Nickel cyclam, molecular catalyst immobilization, multi-walled carbon nanotubes, electrocatalysis

Abstract

Molecular catalysis for selective CO_2 electroreduction into CO can be achieved with a variety of metal complexes. Their immobilization on cathodes is required for their practical implementation in electrolytic cells and can benefit from the advantages of a solid material such as easy separation of products and catalysts, efficient electron transfer to the catalyst and high stability. However, this approach remains unsufficiently explored up to now. Here, using an appropriate and original modification of the cyclam ligand, we report a novel $[Ni(cyclam)]^{2+}$ complex which can be immobilized on carbon nanotubes. This material, once deposited on a gas diffusion layer, provides a novel electrode which is remarkably selective for CO_2 electroreduction to CO, not only in organic solvents but, more remarkably, in water, with faradic efficiencies for CO larger than 90% and current densities of 5-10 $mA.cm^{-2}$ during Controlled potential Electrolysis in H-cells.

Introduction

Molecular catalysis for selective CO_2 electroreduction into CO can be achieved with a variety of metal complexes. The most representative and studied ones are the metal-carbonyl M(bpy=bipyridine)$(CO)_3Cl$ (M=Re, Mn), [Ni(cyclam=1,4,8,11-tetraazacyclotetradecane)]$^{2+}$ and M-porphyrin/phtalocyanine (M=Fe, Co) complexes.[1] The CO_2 reduction reaction (CO_2RR) features kinetic limitations due to the multi-electron and multi-proton transfers, which require the use of catalysts. However, their practical utilization in technological devices such as electrochemical cells requires their fixation, covalent or non-covalent, to the cathode of the cell. Heterogenized molecular catalysts gain the benefits of solid materials, such as facile recovery of products and catalysts, effective electron transport from the electrode support to the catalyst, and high Turnover Numbers, in addition to the typical advantages of molecular complexes, e.g., synthetic control of the electronic properties and the coordination environment of the active sites. This approach has been surprisingly very little explored up to now, and only few complexes have been successfully converted into active electrode materials, as described in recent review articles.[2–4] For example, remarkable performances have been achieved with M-porphyrin/phtalocyanine systems.[5,6] The latter have the advantage of carrying polyaromatic, highly conjugated, macrocyclic ligands which allows direct non-covalent immobilization of the catalyst at the surface of carbon-based electrodes without any

functionalization. In contrast, functional heterogeneization of $M(bpy)(CO)_3Cl$ (M=Re, Mn) and Ni-cyclam catalysts is much more challenging and has been in fact less successful.[7] As a matter of fact, a well-designed functionalization of the ligand is required to promote the adsorption of the catalyst on the carbon-based electrode. Such molecular catalysts can be immobilized using a widely used and straightforward method that relies on hydrophobic and π-π stacking interactions with a carbon-based support, preferably multi-walled carbon nanotubes (MWCNTs), which have the advantages of stability, high electrical conductivity, and large surface areas. The most representative reports concern bipyridine-pyrene derivatives used to immobilize a $[Re(bpy)(CO)_3Cl]$ complex on a graphite support[8] or a $[Mn(bpy)(CO)_3Br]$ complex on carbon nanotubes,[9] however in most cases with limited activity, selectivity and stability, thus low Turnover Numbers.

Recently we addressed the question of immobilizing complexes with non-aromatic ligands on carbon electrodes. For that purpose, we have investigated one of the most studied molecular catalysts for CO_2RR, namely $[Ni(cyclam)]^{2+}$, labelled as Ni-cyclam. Ni-cyclam has attracted a lot of attention in particular for its, almost unique, ability to selectively catalyze the conversion of CO_2 into CO in pure water.[10] C.P. Kubiak and collaborators were first to attempt covalent heterogenization of Ni-cyclam, however with little success.[11] On our side, we recently explored for the first time its non-covalent immobilization on a carbon-based nanostructured electrode using a pyrene functionalization.[12] For that purpose, we synthesized an original pyrene-cyclam derivative and the corresponding Ni complex **A** (Scheme 1), which could be readily attached on CNTs deposited on a gas diffusion layer. The as-prepared electrode proved efficient, selective, robust for electrocatalytic reduction of CO_2 to CO with high turnover numbers and turnover frequencies, however only in aprotic solvent with a very low water content (1%). Larger water content resulted in H_2 production and drastic loss of selectivity for CO.

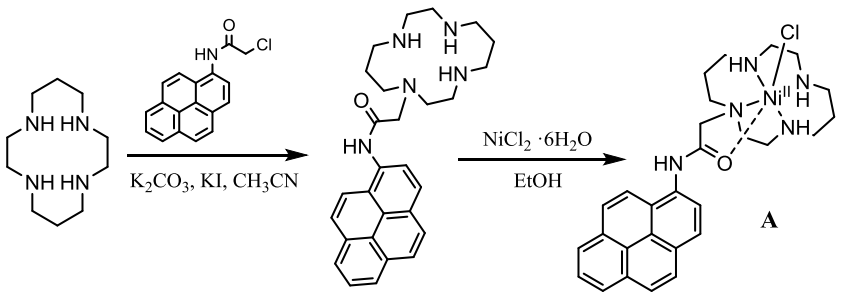

Scheme 1. Synthesis of complex **A**.

However, we showed that this first generation of Ni-cyclam-pyrene catalyst suffered from the following drawbacks. First, the presence of a carbonyl group within the chain linking the cyclam ligand to the pyrene moiety led to a 6-coordinated Ni cyclam complex which is redox active at potentials more cathodic, by 180 mV, than for the unfunctionalized Ni-cyclam. Second, the functionalization of the cyclam ligand had been made on one of the four N atoms, a configuration which was claimed to result in degraded catalytic activity and selectivity, as compared to C-functionalization of cyclam. According to a previous study, the interaction between the cyclam ligand and the electrode surface has a significant influence on the efficiency of Ni-cyclam catalysts. N-functionalization seems to result into increased structural hindrance when attached to the electrode that prevents the ligand to maintain a flat structure which favors selectivity for CO.[11,13] Following our first study, Greenwell and collaborators immobilized a Ni-cyclam-pyrene complex, with an alkyl-pyrene group also attached to a N atom of cyclam (in that case the linker did not carry any carbonyl group), onto a Gas Diffusion Electrode (GDE).[14] While producing CO from CO_2 in a neutral aqueous bicarbonate electrolyte during potential-controlled electrolysis in a flow cell, the system produced large amounts of H_2 and suffered from low stability: the current and selectivity for CO decreased rapidly over time bringing the Faradic Yield (FY) for CO from only 50% to 20% after 3 hours.

To further improve a Ni-cyclam based electrode and get more insights into the requirements for a selective and stable production of CO in aqueous electrolytes, in this report, we describe the synthesis of a novel Ni-cyclam-pyrene complex, named complex **1** (Scheme 2), in which the pyrene substituent was attached to a carbon atom of cyclam. The structure of complex **1** confirmed that Ni is tetracoordinated as in Ni-cyclam, as targeted. Complex **1**, after its immobilization on MWCNTs and deposition on a Gas Diffusion Layer (GDL), is very active, stable and highly selective for CO_2 electroreduction to CO in acetonitrile-water solvent. Interestingly, the novel electrode retains excellent selectivity for CO (FY up to 87%) in aqueous medium, which, to the best of our knowledge, makes this the most selective $[Ni(cyclam)]^{2+}$ catalyst covalently heterogenized on carbon electrodes in water. However, deactivation occurs during electrolysis in water, mainly because poisoning by CO.

Results

Synthesis of ligand L and complex 1

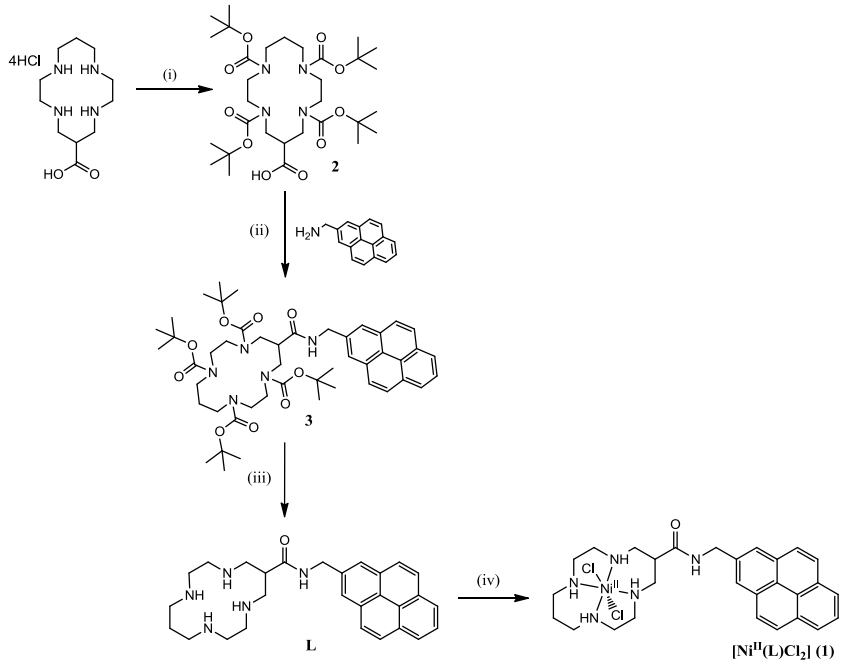

Scheme 2. Synthesis of complex **1.** Conditions: (i) Boc_2O, dioxane, Na_2CO_3, H_2O, RT, 72h, 83%; (ii) EDC-HCl, DMAP, DCM, RT, 5h, 93%; (iii) TFA, DCM, RT, o/n, KOH, H_2O, 100%; (iv) DMF, $NiCl_2 \cdot 6H_2O$, 2h, 49%.

The synthetic steps for the preparation of complex **1** are outlined in Scheme 2. Starting from the commercially available hydrochloride salt of 1,4,8,11-tetraazacyclotetradecane-6-carboxylic acid, the first step involved the protection of the four secondary amines of the cyclam ring with *tert*-butoxycarbonyl (Boc) protecting groups. The cyclam derivative **2** was prepared according to a previously reported procedure with slight modifications.[15] The amide bond formation step took place in dichloromethane, in the presence of the 1-ethyl-3-(3-dimethylaminopropyl)carbodiimide (EDC) and 4-dimethylaminopyridine (DMAP). To maximize the yield, the commercially available salt 1-pyrenemethylamine hydrochloride was pretreated with a base (KOH) and then added to the reaction mixture. The acidic work-up eliminated the unreacted precursors, making it possible to isolate the product in excellent yields (>90%) without the need for additional purification steps before the deprotection step. After evaporation of by-products and solvent, the ligand (**L**) was isolated in the form of trifluoroacetate salt. It has been characterized via IR, ^{1}H NMR, ^{13}C NMR and MS, and its purity was confirmed by elemental analysis (Experimental section). Finally, the ligand was mixed to $NiCl_2 \cdot 6H_2O$ in DMF at room temperature to give complex **1**, which was characterized via elemental analysis, MS and UV-Vis spectroscopy (Experimental section).

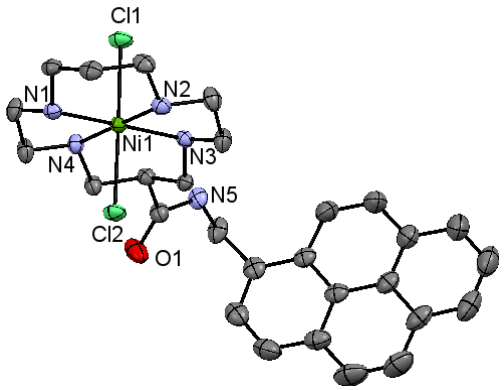

Figure 1. Crystal structure representation of complex **1**. Ellipsoids are drawn with 50% probability. All hydrogen atoms and the two free DMF molecules contained in the asymmetric unit are omitted for the sake of clarity. The crystal is a racemate. Only one of the enantiomers is shown.

Single crystals of complex **1** were obtained as purple plates by slow diffusion of pentane to a DMF solution of the crude product. The molecular structure representation is shown in Figure 1. A summary of the crystal data collection and refinement parameters are listed in Table S1. Selected interatomic bond lengths and angles are listed in Table S2. The nickel ion was found in a distorted octahedral coordination geometry, with two chloride ions occupying two apical positions and the four coordinating nitrogen atoms of the cyclam ring within a plane. The Ni1–N distances ranging from 2.057(2) to 2.066(2) Å and the Ni1-Cl bond lengths (2.485(5) and 2.543(5)Å), are comparable to those found in $[Ni^{II}(cyclam)Cl_2]$.[16]

Homogeneous electrochemical studies of complex 1

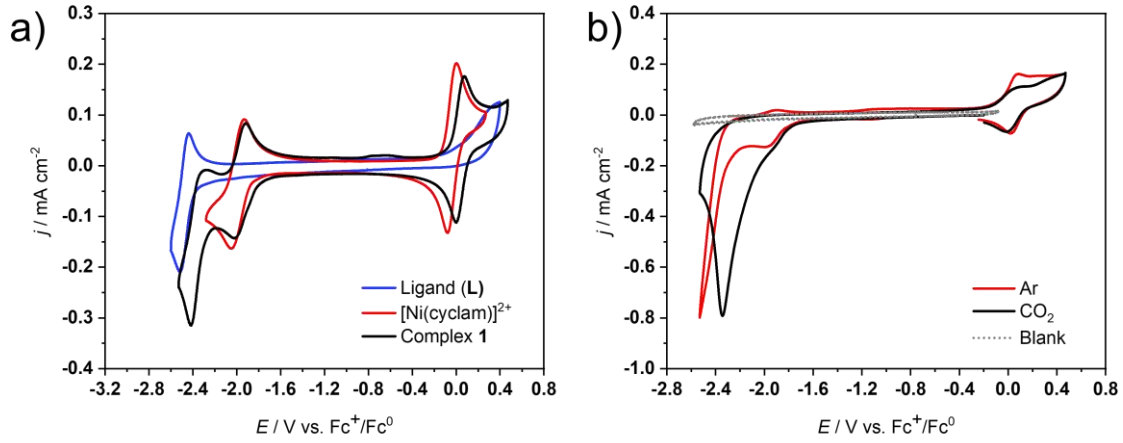

Figure 2. a) CVs of complex **1** (black), $[Ni(cyclam)]^{2+}$ (red), ligand (**L**, blue). Conditions: DMF with 0.1M $TBAPF_6$ as the electrolyte, under Ar and at room temperature. Concentrations were 1 mM for all species. Scan rate 100 mV s^{-1}. b) CV in the absence of complex **1** (blank, grey dotted) and CV of complex **1** (1 mM) in Ar-saturated (red) and CO_2-saturated (black) DMF with 0.1M $TBAPF_6$ at room temperature in the presence of H_2O 2M. Scan rate 100 mV s^{-1}.

The electrochemical properties of complex **1** were studied in DMF with 0.1 M $TBAPF_6$ as a supporting electrolyte. Cyclic voltammograms (CVs) of complex **1** (1 mM) were recorded by using a glassy carbon disk (3 mm diameter) as a working electrode, under an argon atmosphere (Figure 2a). All potentials are reported vs. Fc^+/Fc^0. Scanning towards cathodic potentials reveals a first reversible signal (Figure 2a, black), assigned to the one-electron reduction of Ni^{II} to Ni^{I}, at the same potential, about –2V, as that obtained for the unfunctionalized $[Ni(cyclam)]^{2+}$ complex (Figure 2a, red). A second, more cathodic (-2.4 V), reduction process was assigned to the one-electron reduction of the pyrene moiety, in agreement with the CV of the unmetallated ligand, **L** (Figure 2a, blue). It is interesting to note that this signal in the case of complex **1** is slightly more cathodic and less reversible than that observed for ligand **L**, indicating an effect of the metal ion on the redox properties of the pyrene moiety. Scanning towards anodic potentials shows a reversible signal, assigned to Ni^{II} /Ni^{III} interconversion, also present in the CV of the unfunctionalized $[Ni(cyclam)]^{2+}$ complex. Both cathodic peak current density (j_p) at -2 V and anodic peak current density at -1.9 V varied linearly with the square root of the scan rate ($v^{1/2}$) from 10 to 500 mV s^{-1} r, consistent

with diffusion-controlled processes and thus with active complex **1** remaining in solution (Figure S1), as confirmed by a rinse test (Figure S2).

Upon addition of CO_2 (CO_2-saturated solution) in the presence of H_2O (2 M), it is found that the Ni^{II}/Ni^{I} signal became irreversible and was immediately followed by a catalytic wave at slightly more cathodic potentials, suggesting that complex **1** was able to catalyze CO_2RR (Figure 2b, black). In the absence of CO_2 and with H_2O (2 M), the Ni^{II}/Ni^{I} signal was less affected and a catalytic wave, likely corresponding to proton reduction to hydrogen (HER), occurred at much more negative potentials with an onset potential of -2.3 V (Figure 2b, red). The current density associated with these catalytic processes was dependent on the concentration of water and 2M was chosen for the following of the study as providing the highest current density for CO_2RR (Figure S3), in agreement with the stimulating effect of protons in CO_2RR catalyzed by $[Ni(cyclam)]^{2+}$.[12,17] Even though the foot of the catalytic wave was partly mixed with the Ni^{II}/Ni^{I} feature, the CV indicated an onset potential of about -1.9 V. Considering the potential for the reduction CO_2/CO in a DMF-2M H_2O solvent mixture at -1.41 V vs. Fc^{+}/Fc^{0} (CO_2/CO potential is reported to be - 0.690 V vs. NHE and the Fc^{+}/Fc^{0} potential is reported to be 0.720 V vs. NHE in DMF),[18] the observed onset potential corresponds to a low overpotential of about 490 mV.

Controlled-potential electrolysis (CPE) was performed for 2.2 hours at -2.38 V (Figure S4). The working electrode for the electrochemical cell was a 1 cm^2 GC plate, and the electrolyte was a solution of complex **1** (1 mM) in CO_2-saturated DMF with 0.1 M $TBAPF_6$ and 2 M H_2O as a proton source. Reaction products were analyzed and quantified by gas chromatography (for CO and H_2), ionic exchange chromatography (for HCOOH) and ^1H NMR spectroscopy (for CH_3OH). The current density (0.1 $mA.cm^{-2}$) was stable during the course of the experiment and CO was found to be the only reaction product in the gaseous phase (Faradaic Yield: 96%; 1.8 nmoles) and no formate could be detected in the liquid phase (Figure S4a). As additional evidence of the catalyst stability, a CV recorded after CPE was comparable to that before electrolysis (Figure S4b). CO_2 reduction products were not detected during the same experiment when complex **1** was absent.

Immobilization of complex 1: electrode characterization and CO_2 reduction

Complex **1** was physisorbed on multiwall carbon nanotubes (MWCNTs) through the establishment of π/π-stacking interactions between the pyrene moiety and the carbon material, as described in the experimental section. Briefly, MWCNTs were first sonicated in ethanol in the presence of Nafion and then drop-casted on a commercial gas diffusion layer (GDL). The resulting MWCNTs/GDL assembly was dipped into a methanol solution of complex **1** overnight and, after a washing step in order to remove any unspecifically bound complexes, air-dried before electrochemical experiments.

Scanning Electronic Microscopy (SEM) images of the **1**/MWCNTs/GDL electrode clearly showed the porous network of MWCNTs (Figure S5). X-ray Photoelectron Spectroscopy (XPS) investigation (survey spectrum, Figure S6) indicates the presence of O atoms from alcohol or carboxylic acid defects of pristine MWCNTs along with Ni and N atoms from complex **1** on the surface of the electrode. The N1s and $Ni2p_{3/2}$ signals were observed at 400.4 eV and 855.9 eV, in good agreement with the presence of a Ni^{II} ion and a N/Ni ratio of about 4.5.

CVs were recorded in acetonitrile containing 0.1M $TBAPF_6$, using the as-prepared **1**/MWCNTs/GDL electrode (Figure S7). The high capacitive currents observed in the voltammograms are explained by the 3D structure of the working electrodes but a signal at approximately -2 V vs. Fc^+/Fc^0 was observed, likely corresponding to the one-electron reduction of Ni^{II} to Ni^{I}, in good agreement with the presence of the immobilized catalyst. The integration of the reduction signal at around -2 V at 20 mV s^{-1} (in agreement with the one-electron reduction of Ni^{II} to Ni^{I} previously observed for complex **1**) allowed to get an evaluation of the number of active sites of 4.2 10^{-9} mol cm^{-2} (Experimental section). Such a value is consistent with previously reported values for molecular catalysts deposited on MWCNTs. [9,19]

Linear sweep voltammograms (LSVs), obtained with the new electrode in CO_2–saturated CH_3CN containing 0.1M $TBAPF_6$ as the electrolyte, in the presence of 1% H_2O, shows a catalytic wave occurring at about – 2.0 V and assigned to CO_2 reduction (Figure 3a). A second wave occurred at about 300 mV more cathodic potentials, likely accounting for Hydrogen Evolution reaction (HER). Indeed, the same feature at comparable potentials was

observed in the absence of CO_2 with a MWCNTs/GDL and a **1**/MWCNT/GDL electrode (Figure 3a and S8a) as well as with a MWCNTs/GDL electrode in the presence of CO_2 (Figure S8a), thus pointing to the MWCNTs/GDL support as the promoter of selective production of H_2.

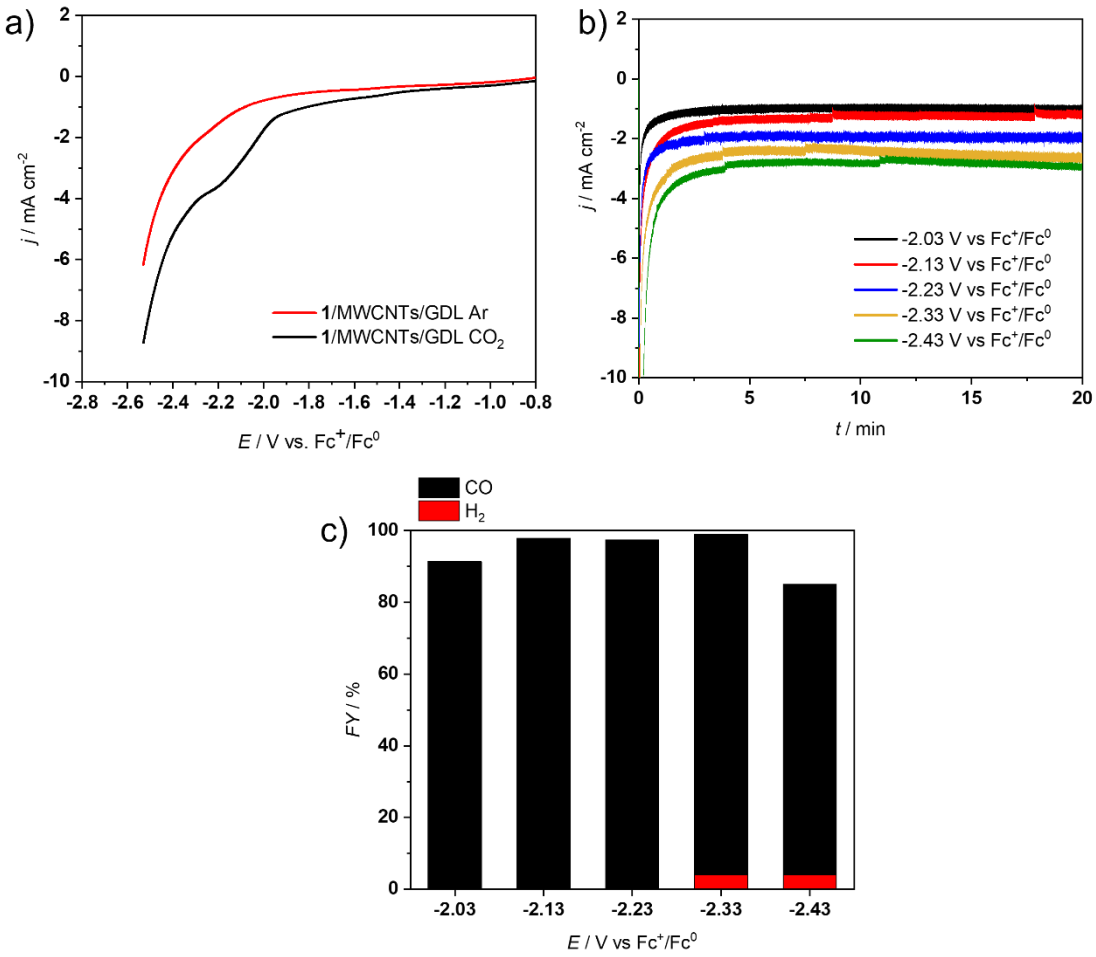

Figure 3. (a) LSV of **1**/MWCNTs/GDL in acetonitrile with $TBAPF_6$ 0.1 M and H_2O 1% under CO_2 or Ar. Scan rate 10 mV s^{-1}. (b) Controlled Potential Electrolysis using **1**/MWCNTs/GDL as the electrode at different potentials under the same conditions. (c) Faradaic yields for CO and H_2 after 20 min electrolysis at different potentials under the same conditions with **1**/MWCNTs/GDL. The amounts in nanomoles are given in Table S3.

Controlled Potential Electrolysis (CPE) was carried out at various potentials from – 2.03 to – 2.43 V vs. Fc^+/Fc^0 for 20 min (Figure 3b). The current densities were stable at all potentials. Without any activity loss, the same electrode could be utilized in multiple separate electrolysis tests. Figure 3c depicts the range of CO_2 reduction products in terms of faradaic yields (FY). CO was the major product at all potentials, and in particular it was the only product detected between -2.03 and -2.23 V. H_2 appeared at more cathodic potentials but

accounted for only a few %. Based on LSV data discussed above we assign this production to HER promoted by the MWCNTs/GDL support. No formate could be found in all tests. CPE employing a MWCNTs/GDL electrode was carried out at - 2.13 V vs. Fc^+/Fc^0 for 20 min as a control experiment (Figure S8b). In addition to having a significantly lower current density, the system was also selectively producing H_2 (FY > 80%).

The stability of the catalytic material and its selectivity were confirmed by a long-term (4h) electrolysis carried out at - 2.23 V vs. Fc^+/Fc^0 using the **1**/MWCNTs/GDL electrode. The FY for CO was more than 90% after the 4h electrolysis (Figure S9). No formate could be detected. SEM analysis revealed that the electrode structure had not changed after 4h electrolysis (Figure S5). A Turnover Number (TON) for CO generation of 14630 was determined based on the quantity of electroactive sites on the electrode's surface ($4.2\ 10^{-9}$ mol cm^{-2}), which corresponds to a Turnover Frequency value of 1.01 s^{-1} (after 4h electrolysis).

Electroreduction of CO_2 catalyzed by 1/MWCNTs/GDL in water

The novel electrode material was tested for the electrochemical reduction of CO_2 in water containing 0.1 M $KHCO_3$ as the electrolyte, under a constant flux of CO_2 (5 ml/min). Interestingly, a linear sweep voltammogram (LSV) showed a catalytic wave occurring at more anodic potentials than that observed either with the MWCNTs/GDL control electrode or with the **1**/MWCNTs/GDL electrode in the absence of CO_2 (Figure 4a). This suggested a selective CO_2 reduction catalysed by complex **1** immobilized on the electrode at potentials between –0.52 (the onset potential resulting in an overpotential of about 400 mV) and -0.8 V vs RHE and HER occurring at more cathodic potentials. The fact that the LSVs of the MWCNT/GDL electrode, with and without CO_2 (Figure S10a) and of the **1**/MWCNTs/GDL electrode in the absence of CO_2 (Figure 4a) are comparable suggests that HER is essentially due to catalysis by the MWCNTs/GDL support.

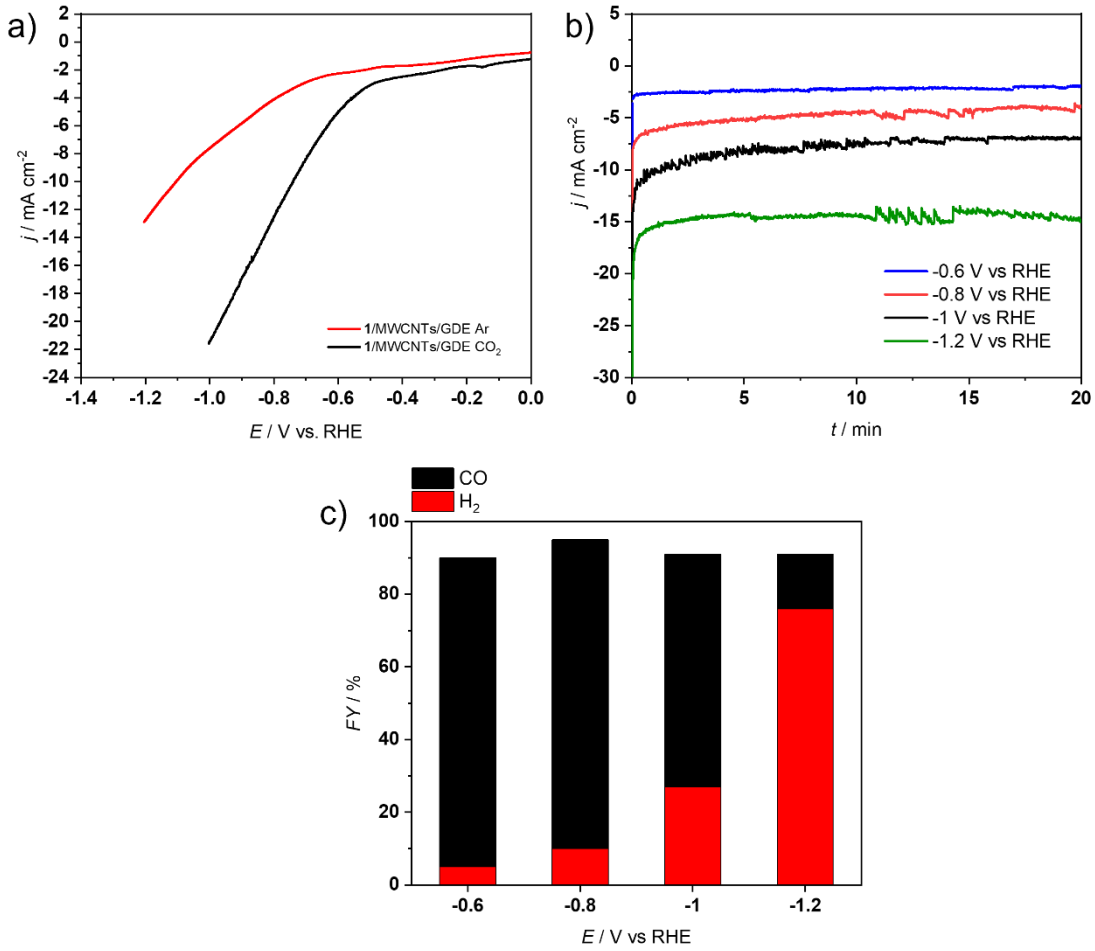

Figure 4. (a) LSVs of **1**/MWCNTs/GDL (black and red) and MWCNTs/GDL (dotted) in water with $KHCO_3$ 0.1 M under CO_2 or Ar. Scan rate 50 mV s^{-1}. (b) Controlled Potential Electrolysis using **1**/MWCNTs/GDL as the electrode at different potentials under the same conditions. (c) Faradaic yields for CO and H_2 after 20 min electrolysis at different potentials under the same conditions with **1**/MWCNTs/GDL. The amounts in nanomoles are given in Table S4.

During CPE experiments carried out at various potentials from – 0.6 to – 1.2 V vs. RHE for 20 min (Figure 4b), the current density proved stable (occasional noise was likely caused by gas bubbles developing at the surface of the electrode). Figure 4c depicts the range of CO_2 reduction products in terms of faradaic yields (FY). CO was the major product between -0.6 and -1 V, with the highest FY_{CO} values (about 85%) between – 0.6 and -0.8V vs. RHE (with a current density of 5 mA.cm^{-2} at – 0.8 V vs RHE) and FY_{H2} below 10%. At more cathodic potentials, as anticipated (see above), H_2 production increased and H_2 was found to be the major product (FY_{CO} =20%; FY_{H2}=80%) at -1.2 V. No formate could be found in all tests. CPE employing a MWCNTs/GDL electrode was carried out at – 0.8 V vs. RHE for 20 min as a control experiment (Figure S10). In addition to having a lower current density (~2.5 mA.cm-

^{2}), H_2 was almost the only reaction product (only traces of CO were detected). This confirmed that the HER was essentially due to the activity of the MWCNTs/GDL support.

During a longer experiment (4h) carried out at – 0.8 V vs. RHE using the **1**/MWCNTs/GDL electrode, CO was the major product (1043.6 nmoles and TON= 248 after the first hour). However, the system experienced a decay of current density during the first three hours (from around 6 mA cm^{-2} after 20 min CPE to a plateau value of 2.6 mA cm^{-2}) and a loss of selectivity (with a FY for CO of 87 and 53% after 20- and 200-min electrolysis, respectively) (Figure 5). Nevertheless, the XPS spectrum of the electrode after 4 hours electrolysis was comparable to that before electrolysis, showing the presence of Ni with a Ni:N ratio of about 4.8 (Figure S11). In agreement with CO inactivating the system, when electrolysis was carried out under the same conditions but in the presence of 5% CO, the current density decayed much more rapidly and the FY for H_2 reached higher values at shorter reaction times (Figure S12).

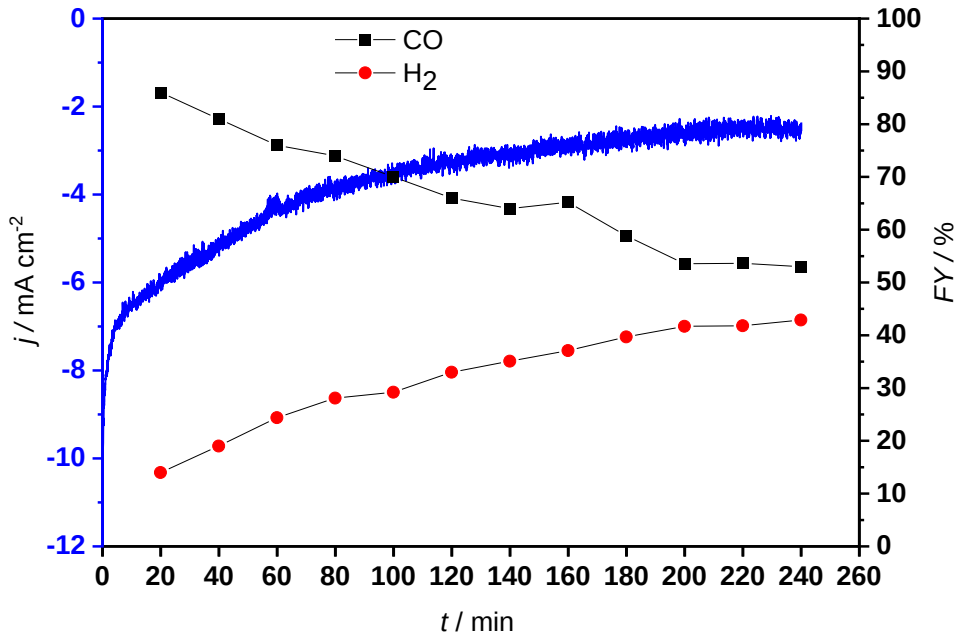

Figure 5. Controlled-Potential Electrolysis at -0.8 V vs. RHE using **1**/MWCNTs/GDL in water with 0.1M $KHCO_3$ and a CO_2 flow rate of 5 ml/min (blue). Faradaic yields for CO (black) and H_2 (red) during the same experiment. The amounts in nanomoles are given in Table S5.

Catalyst regeneration

A likely origin of catalyst inactivation is the formation of Ni-carbonyl complex, derived from the reaction of Ni^{I} with CO, a process well established in previous studies [17,20,21]. In order to verify this hypothesis, a long-term electrolytic experiment (Figure 6a) was followed by an oxidative treatment (at 0.79 V vs RHE for 10 minutes) of the electrode used to de-coordinate CO from the complex and the treated electrode used for a second electrolytic run (Figure 6b). Indeed, unlike Ni^{I}, Ni^{II} is known not to spontaneously coordinate CO.[17] As shown in Figure 6, it was found that the oxidative treatment allowed the electrode to regain its initial activity: not only the current density obtained during the second run (Figure 6b) was comparable to that obtained during the first run (Figure 6a) but also the FY_{CO}, while at 72% after the first run, was at 87 % at the beginning of the second run, identical to that at the beginning of the first run, before subsequent loss of CO selectivity following the same kinetics. These experiments thus nicely show that the inactivation of the complex in water is fully reversible. While some release of complex **1** cannot be excluded, this experiment also shows that the amount of catalytically active species at the surface of the electrode remains stable during catalysis.

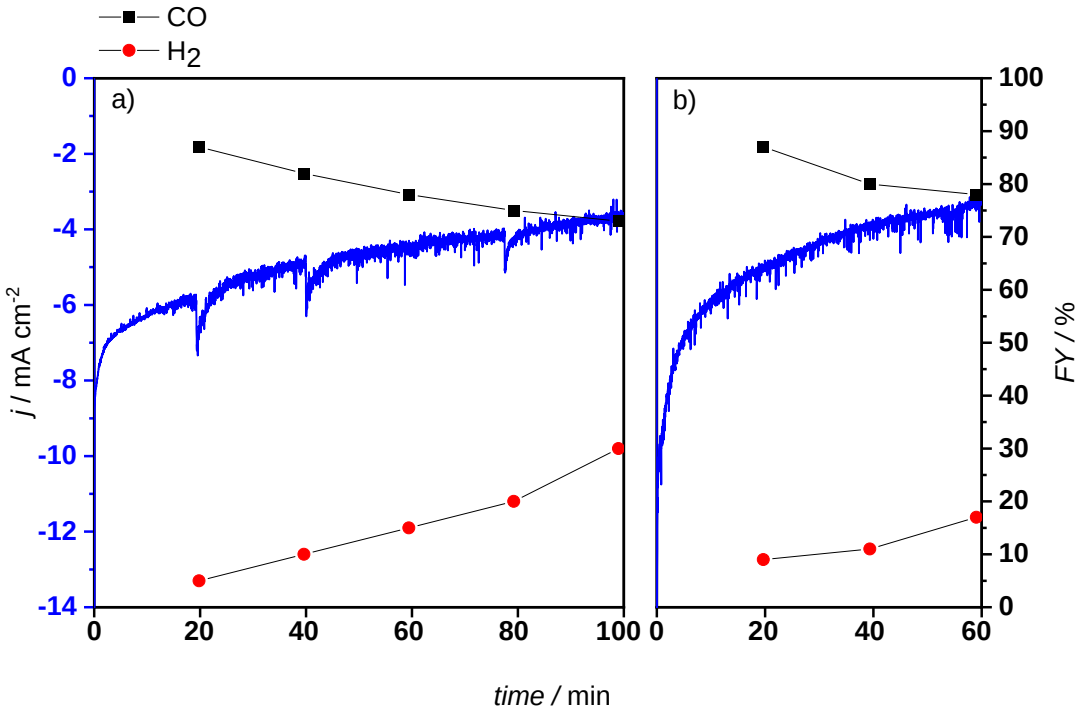

Figure 6. a) Controlled-Potential Electrolysis at -0.8 V vs. RHE using **1**/MWCNTs/GDL in water with 0.1M $KHCO_3$ and a CO_2 flow rate of 5 ml/min (blue). Faradaic yields for CO (black) and H_2 (red) during the same experiment; b) Controlled-Potential under the same conditions using **1**/MWCNTs/GDL from a), after having applied an oxidative potential (0.79 V vs RHE) for 10 minutes (blue). Faradaic yields for CO (black) and H_2 (red) during the same experiment. The amounts in nanomoles are given in Table S6.

Computational studies

Density Functional Theory (DFT) calculations, detailed in the Supplementary Information section, were conducted to further validate the electrochemical properties of complex **1**. The calculations support that the first reduction of **1** corresponds to the conversion of Ni^{II} to Ni^{I}. In water, this reduction was calculated to occur at a potential of -0.30 V vs. RHE, very close to that calculated for the unmodified Ni-cyclam complex (-0.41 V vs. RHE). According to previous computational investigations, the potential-determining step for the CO_2RR corresponds to a proton-coupled electron transfer (PCET) to generate the Ni^{II}-COOH intermediate from the formal Ni^{II}-$CO_2^{\bullet-}$ species.[17] For **1**, the calculated reduction potential for this step was -0.74 V vs RHE, taking CO_2 + H_2O as the source of protons, as previously done by Song et al.[17] This value is in rather good agreement with the experimental position of the catalytic wave (Figure 4a), suggesting that the immobilization of the catalyst onto the

MWCNTs/GDL electrode did not significantly influence its catalytic properties. Of note, periodic DFT calculations revealed that the electronic structure of **1** is only scarcely affected by immobilization (Figure S13-S15), which further justifies the use of a discrete molecular model to investigate the catalytic properties of complex **1** in water.

Next, the ability of **1** to catalyze HER under the experimental conditions was evaluated. Previous experimental studies suggested the participation of a Ni^{III}-H hydride,[22] resulting from the protonation of the Ni^{I} species, as the key intermediate from which HER takes place. A pK_a value of 3.3 for the Ni^{III}-H in the case of complex **1** was calculated, being in line with the experimental value of 1.8 measured for Ni-cyclam.[23] This clearly indicates that the protonation of Ni^{I} is unlikely under the neutral pH conditions used in this study. Furthermore, the calculated pK_a for a putative Ni^{II}-H intermediate was 26.4, but its formation from Ni^{I} through a PCET process requires a reduction potential of -1.07 V vs. RHE (Scheme S1), which is more negative than that required for HER promoted by the MWCNTs/GDL support (Figure 4a). Similarly, the sequential reduction of Ni^{I} and protonation of the resulting Ni^{I} with an extra electron delocalized over the pyrene ring involves an excessively demanding electron transfer process (-1.73 V vs. RHE, Scheme S1). Altogether, our calculations nicely establish that complex **1** is unlikely to promote HER under our experimental conditions, in excellent agreement with the electrochemical data and our assignment of observed HER to the activity of the MWCNTs/GDL electrode (see above).

Finally, to further understand the decrease of CO production rate with time (Figure 6), additional calculations were carried out to explore the possible inhibition of the catalytic sites by the CO product.[17,20] Indeed, the coordination of CO to the Ni^{I} intermediate is exergonic by 2.5 kcal mol^{-1}, indicating that CO competes with CO_2 for coordinating the electrochemically generated Ni^{I} sites. Thus, as the concentration of CO increases, that of bare Ni^{I} sites available for CO_2RR decreases, explaining the overall decrease in current density and Faradaic yield for CO. Conversely, the binding of CO to the Ni^{II} species is endergonic by 4.3 kcal mol^{-1}, in agreement with the experimental reactivation of the catalyst upon reoxidation of the Ni^{I} to Ni^{II}.

Discussion

By introducing, for the first time, the pyrene substituent on a carbon atom of the cyclam ligand, a novel Ni-cyclam derivative, complex **1**, which has retained the stereo-electronic properties of the parent Ni-cyclam complex, was successfully synthesized. This was attained by functionalizing the cyclam ring in a position that, unlike N-functionalized derivatives, does not allow the carbonyl group of the linker to coordinate the Ni center and does not alter N-H groups. This is clearly shown from the three-dimensional structure of complex **1** and from the redox potential value of the Ni^{II}/Ni^{I} couple, which is identical to that of the Ni-cyclam complex. The **1**/MWCNTs/GDL electrode, obtained by immobilization of complex **1** on MWCNTs and deposition on a GDL, proved highly active for CO_2RR, stable and selective for CO production (with a FY > 95%) in organic solvent in the presence of a small amount of water (1%) as a source of protons, within a potential range of about 300 mV below the catalytic onset potential. At potentials more cathodic than about – 2.4 V vs Fc^{+}/Fc^{0}, the MWCNTs/GDL support becomes active for HER catalysis, explaining the production of H_2 below that potential. With an impressive TON of 14630 after 4 h electrolysis, this system is among the best immobilized molecular catalysts for CO_2 to CO conversion in organic solvent[2,4,7].

More interestingly, the **1**/MWCNTs/GDL electrode is also remarkably selective for CO production in purely aqueous electrolyte. CO_2 reduction to CO occurs with FY close to 90% during a short-term (20 minutes) electrolysis within a 200-mV potential range (from about -0.6 to -0.8 V vs RHE). Only when potentials more cathodic than -0.8 V vs RHE were applied, HER, promoted by the MWCNTs/GDL support, became important and then predominant at potentials below -1.0 V. Comparable systems with immobilized molecular catalysts within H-cells using aqueous electrolytes with such high selectivity for CO_2 reduction to CO and relatively high current densities (5-10 $mA.cm^{-2}$) are exceedingly rare.[19,24,25] The **1**/MWCNTs/GDL electrode thus compares well with the best systems based on Co(quaterpyridine) or Co(phtalocyanine) complexes immobilized on MWCNTs displaying current densities of 10-20 $mA.cm^{-2}$ and high selectivity for CO (FY=90%).[24,25]

It is worth noting on the mechanistic consideration that Ni-cyclam is not able to catalyze proton reduction under neutral conditions, at least at moderately cathodic potentials (between -0.6 and -0.8 V vs. RHE) employed for long-term CPE, and this is why it is selective for CO

production. This is consistent with DFT calculations and with the calculated pK_a value of 3.3 for the Ni^{III}-H hydride species (experimentally determined as 1.8 for unfunctionalized Ni-cyclam[20]). Indeed, the mechanism of this catalyst implies an initial reduction of Ni^{II} into Ni^{I} which is accompanied by CO_2 binding and then proton-coupled electron transfer promoting C-O bond cleavage upon further protonation yielding CO and water. Based on the pK_a value of Ni^{III}-H, Ni^{I} is not basic enough to get protonated and, furthermore, our calculations reported here indicated that further reduction of the Ni^{I} species would request too negative potentials. Therefore, on this basis and on the results presented here, it is likely that the observed formation of H_2 in Ni-cyclam systems as coming exclusively from the activity of the carbon support and not from a supposed HER activity of the molecular catalyst. This then nicely explains the major difference between our previous complex **A** and present complex **1** regarding CO_2RR activity in water.[12] With a catalytic wave shifted cathodically (onset – 0.7 V for complex **A** vs – 0.5 V for complex **1**), CO_2RR catalyzed by complex **A** cannot compete efficiently with HER promoted by the MWCNTs/GDL support. A gas diffusion electrode with an analog of complex **A** developed by Greenwell and collaborators gave also much less selective CO production (FY = 50 %) in water.[14] Previous reports discussing the CO:H_2 selectivity in the case of Ni-cyclam and derivatives have rarely considered this possibility of the involvement of the electrode carbon support *and not Ni-cyclam* for HER. That the carbon electrode is a good HER catalyst allowing HER to compete with CO_2RR catalyzed by Ni-cyclam in solution has been for example discussed by C.W. Machan and collaborators.[21]

Finally, we observed an inactivation of the **1**/MWCNTs/GDL electrode, resulting in HER from the MWCNTs/GDL support becoming dominant, during CPE in water. This was clear from a decrease of FY_{CO}, an increase in FY_{H2} and a decrease of current density as a function of time. It can be assigned to the well-established formation of nickel carbonyl complexes.[17,20,26] While problematic, it is interestingly observed that the catalyst could be easily reactivated for subsequent electrolysis. This reversibility opens the possibility to develop further this novel electrode with further investigation of technological strategies to avoid the formation of the Ni-CO complex and/or to reactivate the catalyst, as previously proposed.[20] During the course of this study, Siritanaratkul and collaborators reported a zero gap electrolyte-free electrolyzer using a bipolar membrane and a gas diffusion cathode, on which Ni(cyclam) complex was deposited. While the system was less selective for CO_2 reduction, it also enjoyed reversible inactivation during electrolysis, mainly assigned to the formation of a nickel-carbonyl complex.[27]

In conclusion, the present study provides a further step forward in the utilization of the molecular $[Ni(cyclam)]^{2+}$ complex as a catalyst for CO_2 electroreduction. By an appropriate an original functionalization of the ligand and an immobilization of the modified Ni complex, using the pyrene-CNT approach, an active and selective electrode has been prepared for CO formation in aqueous electrolytes. Further investigation is required to improve the stability of this novel electrode. The molecular nature of the electrode opens possibilities for improving its performances by further synthetic modifications of the ligand.

Experimental Section

General

All starting materials were commercially available (Sigma, Acros Organics, Alfa Aesar and TCI) and were used without further purification. 1,4,8,11-tetraazacyclotetradecane-6-carboxylic acid was purchased from Chematech. Diethylether (Et_2O), tetrahydrofuran (THF), toluene and dichloromethane (DCM) were dried with an MBraun solvent purification system and stored under argon. All reactions were carried out under Ar atmosphere unless specified. TLC detection was accomplished by irradiation with a UV lamp at 265 or 313 nm. Organic solutions were concentrated under reduced pressure on a Büchi rotary evaporator. Yields refer to purified compounds, unless otherwise stated. Melting points were determined on a Büchi B-545 device.

^{1}H and ^{13}C NMR spectra were recorded on a 400 MHz NMR JEOL spectrometer (500 and 101 MHz for ^{1}H and ^{13}C respectively), at room temperature unless specified, and are referenced either to tetramethylsilane (TMS) peak (at δ 0 ppm), or internally referenced to residual solvent signals, $CDCl_3$ referenced at δ 7.26 and 77.16 ppm.

Data for ^{1}H is reported as follows: chemical shift (δ ppm), multiplicity (s = singlet, d = doublet, t = triplet, q = quartet, m = multiplet), coupling constant (Hz), integration and assignment. Data for ^{13}C are reported in terms of chemical shift, multiplicity (s = singlet, d = doublet, t = triplet, q = quartet, m = multiplet), coupling constant (Hz) and no special nomenclature is used for equivalent carbons.

UV-Vis spectra were recorded using a Agilent Cary 100 UV-Vis spectrophotometer. IR spectra were recorded on a Perkin Elmer Spectrum 65 FT IR Spectrometer and are reported in terms of frequency of absorption (cm^{-1}).

High-resolution mass spectra were obtained using ESI ionization on a Bruker Maxis Impact mass spectrometer.

*Synthesis of Complex **1***

1,4,8,11-tetrakis(tert-butoxycarbonyl)-1,4,8,11-tetraazacyclotetradecane-6-carboxylic acid (2): This protocol is modified from prior disclosed conditions.[15] 1,4,8,11-tetraazacyclotetradecane-6-carboxylic acid (0.1 g, 0.26 mmol) and Na_2CO_3 (0.138 g, 1.30 mmol, 5.1 eq) were dissolved in H_2O (2.50 mL) and the solution was stirred for 10 minutes. Boc_2O (0.268 g, 1.23 mmol, 4.8 eq) in dioxane (2.50 mL) was added to this solution dropwise, and the reaction mixture was stirred at room temperature and monitored by TLC (R_f 0.5, EtOAc). After 72h, the solution was concentrated under vacuum to remove the dioxane. The aqueous phase was first extracted with Et_2O, then acidified with H_2SO_4 3M to pH 1.0–2.0. The aqueous phase was then extracted with Et_2O/EtOAc (1:3). The organic layer was collected, washed twice with brine and water, dried over $MgSO_4$, and finally evaporated under vacuum. The product was obtained as a white solid with a glassy texture and was used without need of further purification. (0.137 g, yield 83%). Melting point: 69°C.

IR (neat, ATR) $\tilde{\nu}$ /cm^{-1}: 3000, 2950, 2800, 1700, 1490, 1480,1400

^{1}H NMR (400 MHz, $CDCl_3$, 55°C) δ 1.46 (s, 36H), 1.69-1.84 (m, 3H), 2.90 (t, 1H), 3.13-3.31 (m, 4H) 3.33-3.54 (m, 8H), 3.56-3.66 (m, 4H).

1-Pyrenemethylamine: 1-Pyrenemethylamine hydrochloride (0.1 g, 0.38 mmol) was stirred in CH_2Cl_2 (10 mL) and KOH 2M (10 mL) for 2 hours. The organic layer was then collected, dried over $MgSO_4$ and finally evaporated under vacuum to give the amine in a quantitative yield (0.9 g, yield 100%). Melting point: 172-173°C.

IR (neat, ATR) $\tilde{\nu}$ /cm^{-1}: 3000, 2861, 2500, 1586, 1495

^{1}H NMR (400 MHz, $CDCl_3$) δ 4.61 (s, 2H), 7.99-8.07 (m, 4H), 8.14-8.20 (ddd, J =13.3, 8.4, 5.0 Hz 4H), 8.35 (d, J =9.2 Hz, 1H).

Tetra-tert-butyl 6-((pyren-2-ylmethyl)carbamoyl)-1,4,8,11-tetraazacyclotetradecane-1,4,8,11 tetracarboxylate (3): This protocol was modified from prior disclosed conditions.[28] A flame-dried round-bottomed flask was degassed, flushed with argon, and charged with 2mL DCM, EDC-HCl (1-(3 dimethylaminopropyl)-3-ethylcarbodiimide hydrochloride, 0.039g, 0.2 mmol, 1.3 eq), and DMAP (0.21 mmol, 1.4 eq, 0.026g). The reaction flask was cooled to zero degrees in an ice bath. **2** (0.1 g, 0.15 mmol) was dissolved in 1 mL DCM and added to the previous mixture. After five minutes of stirring, 1-pyrenemethylamine (0.036g, 0.15 mmol, 1 eq) was dissolved in 1 mL DCM and added to the mixture. The ice bath was removed, the reaction was monitored via TLC (R_f 0.5, EtOAc:hexane 50:50) and allowed to stir overnight at RT. The reaction was then quenched with 4 mL 1M HCl and the organics separated. The aqueous layer was extracted three times with $CHCl_3$. All the organic layers were combined and dried over $MgSO_4$ and evaporated under vacuum. The crude product (0.12g ,93%) was used for the next step without purification. Melting point: 114-115°C.

IR (neat, ATR) $\tilde{\nu}$ /cm^{-1}: 3000, 2900, 1700, 1550, 1475, 1300

^{1}H NMR (400 MHz, $CDCl_3$): δ 8.29 (d, J = 9.3 Hz, 1H), 8.15 (ddd, J = 13.0, 7.7, 3.6 Hz, 4H), 8.08 – 7.91 (m, 4H), 5.12 (d, J = 5.1 Hz, 2H), 3.63 (d, J = 6.4 Hz, 4H), 3.55 – 3.32 (m, 9H), 3.22 (dd, J = 32.0, 9.9 Hz, 4H), 2.94 – 2.72 (m, 1H), 1.77 (dt, J = 13.4, 6.6 Hz, 2H), 1.38 (d, J = 19.6 Hz, 36H).

HR-MS (ESI) exact mass calculated for $[M+H]^+$ ($C_{48}H_{68}N_5O_9$) 858.49; found 858.50.

N-(pyren-2-ylmethyl)-1,4,8,11-tetraazacyclotetradecane-6-carboxamide (L): The procedure was modified from previously described conditions.[29] In a round-bottom flask, **3** (0.2g, 0.23 mmol), TFA (1.48g, 13.5 mmol, 56 eq) and 5 mL DCM were stirred under argon overnight at room temperature. Successively, the mixture was evaporated under vacuum. The orange solid that remained was dissolved in 0.5 mL water. KOH 2M was added until pH was 11-12. The mixture was stirred for 30 minutes, then the aqueous layer was extracted with $CHCl_3$ (three times). The organic layer was washed with water once, then dried over $MgSO_4$ and evaporated under vacuum to yield an off-white powder (0.1 g, 100% yield). Melting point: 189-190°C.

IR (neat, ATR) $\tilde{\nu}$ /cm^{-1}: 3259, 3192, 3033, 2198, 2869, 2807, 1631, 1461, 1120, 839.

^{1}H NMR (400 MHz, $CDCl_3$) δ 10.19 (s, 1H), 8.32 (d, J = 9.2 Hz, 1H), 8.24 – 8.12 (m, 4H), 8.09 – 7.98 (m, 4H), 5.19 (d, J = 5.2 Hz, 2H), 3.12 (dd, J = 11.2, 4.3 Hz, 2H), 2.80 (dd, J = 11.3, 2.3 Hz, 2H), 2.65 – 2.33 (m, 9H), 2.12 (dt, J = 18.2, 7.0 Hz, 4H), 1.53 – 1.43 (m, 2H).

^{13}C NMR (101 MHz, $CDCl_3$) δ 174.18 (s), 132.60 (s), 131.43 (s), 130.99 (d, J = 14.5 Hz), 128.86 (s), 128.04 (s), 127.49 (d, J = 8.1 Hz), 126.80 (s), 126.19 (s), 125.56 – 125.00 (m), 124.95 (s), 123.14 (s), 51.69 (s), 50.66 (s), 49.03 (d, J = 18.1 Hz), 45.52 (s), 41.50 (s), 29.33 (s).

HR-MS (ESI) exact mass calculated for $[M+H]^+$ ($C_{28}H_{36}N_5O$) 458.28; found: 458.29.

Complex $[Ni^{II}(L)Cl_2]$ (1): L (0.071 g, 0.16 mmol) and $NiCl_2{\cdot}6H_2O$ (0.037 g, 0.16 mmol) were mixed in 2 mL DMF. The solution turned pink after 10 minutes. After stirring 2h at room temperature, a pink precipitate formed. The precipitate was recuperated, washed with EtOH and Et_2O, and dried under vacuum. (44.5 mg, 49 %).

UV-Vis [MeOH]: λ nm (ε, M^{-1} cm^{-1}): 543 (10.7), 389 (1880), 353 (10920), 343 (15000), 329 (10000), 277 (16300), 266 (11060), 241(32600), 232 (22120).

HRMS (ESI) m/z: $[M-Cl]^+$ Calcd 550.1884. Found 550.1880.

Single crystals suitable for X-ray diffraction were obtained from slow diffusion of pentane in DMF containing **1.** CCDC 2167708 contain the supplementary crystallographic data for this study.

Elemental analysis calcd. for 2[$\mathbf{Ni^{II}(L)Cl_2}$]**.**EtOH: % C 57.08, H 6.28, N 11.48; found % 57.00, H 5.82, N 10.97 (the small differences are most likely due to some decomposition with temperature during sample transport).

Homogeneous Electrochemical Studies

A VSP300 potentiostat (Bio-Logic Science Instruments SAS) was used for all electrochemical studies, which were carried out in N,N-Dimethylformamide (DMF) at room temperature. The supporting electrolyte was 0.1 M tetrabutylammonium hexafluorophosphate ($TBAPF_6$). A three electrode configuration was used for the cyclic voltammetry (CV) experiments. The working electrode, a 3 mm diameter glassy carbon (GC) electrode, was polished on a polishing cloth with a 1 µm diamond suspension (Struers), sonicated for 10 seconds, thoroughly rinsed with ethanol, and dried before the experiments. A counter electrode made

of platinum wire was employed (after being flame-annealed). The reference electrode (Ag/AgCl in a saturated KCl solution) was equipped with a bridge to enable operation in organic solvent. As an internal standard, the ferrocene/ferrocenium ($Fc^{+/}Fc^{0}$) redox couple was added at the conclusion of each measurement and used to calibrate all potentials ($E_{1/2}$ (Fc^{+}/Fc^{0}) in DMF = 0.60V vs. Ag/AgCl/sat. KCl). Only the second cycle of each CV is displayed (there was no variation between successive scans). Two ceramic-PVDF composite membranes (16 m thick, Xuran) separating the anodic and cathodic compartments were used in a gas-tight, two-compartment electrochemical cell for controlled potential electrolysis (CPE) tests. A 1 cm^2 glassy carbon plate was employed as the working electrode, while a platinum mesh served as the counter electrode and an Ag/AgCl electrode in a saturated KCl solution (equipped with a bridge to enable operation in organic solvents) was used as the reference electrode. DMF was the solvent, 2 M of water the proton source and 0.1 M of $TBAPF_6$ the electrolyte in both anolyte and catholyte. 1 mM of complex **1** was added to the catholyte. Before beginning the electrolysis, the compartments were saturated with CO_2 for at least 20 minutes, but no additional gas was bubbled during the experiment. The total volume of the cathode side of the cell was 22.6 mL, with approximately 10.6 mL of headspace volume. Gas products were measured from 50 µL aliquots of the headspace of the cathode compartments via gas chromatography (8610C, SRI Instruments). Thermal conductivity detectors (TCD) and flame ionization detectors (FID) were used to identify hydrogen (H_2) and carbon monoxide (CO), respectively. An ionic exchange chromatograph (Metrohm 883 Basic IC) equipped with a Metrosep A Supp 5 column and a conductivity detector was used to assess liquid products.

The products in the head-space gas of the cathodic side were quantified to determine the faradaic yields following Equation 1:

$$Faradaic\ efficiency = \frac{N \times F \times n}{Q} \times 100 \quad (1)$$

Where N, F and Q represent the number of moles of H_2/CO produced, the Faraday's constant (C mol^{-1}), and the charge passing through the system (C), respectively. Due to the fact that the reaction required 2 moles of electrons to make 1 mole of product, n is equal to 2.

Electrodes preparation and characterization

A 3 cm x 1 cm gas diffusion layer (GDL, AVCarb GDS 3250, Fuel Cell Store) strip was used as the electrode and was quickly sonicated in EtOH before being allowed to dry in air.

MWCNTs (Sigma) underwent acid treatment (they were dispersed in H_2SO_4 2 M, sonicated for 1 hour at room temperature, repeatedly rinsed with H_2O, then EtOH, and dried overnight in a vacuum oven at 70°C). Successively, 2 mg of the dried MWCNTs were sonicated with ethanol (200 µl) containing a solution of Nafion perfluorinated resin (5 µl of a 5 wt% solution in a mixture of lower aliphatic alcohols containing 5% water) for at least 30 minutes. This suspension was then drop-cast onto the GDL (1 cm^2 deposit) and allowed to dry for at least 30 minutes in air at 70°C. The GDL-MWCNTs electrode was then submerged in a solution of complex **1** in DMF (10 mM) overnight. The electrode was then dried, washed with acetonitrile and water, then dried in the air.

SEM images were acquired using a Hitachi S-4800 scanning electron microscope. X-ray photoelectron spectra (XPS) were collected using a Thermo Electron Escalab 250 spectrometer with a monochromated Al Ka radiation (1486.6 eV). The analyzer pass energy was 100 eV for survey spectra and 20 eV for high resolution spectra. The analysed area was 500 mm^2. The photoelectron take-off angle (angle between the surface and the direction in which the photoelectrons are analysed) was 90°.

Equation 2 was used to determine the number of electroactive sites by the integration of the reduction wave in the CV scan (Figure S7):

$$\Gamma Ni = \frac{q}{nFA} \quad (2)$$

Where ΓNi is the number of electroactive sites (mol cm^{-2}), q is the charge (C)obtained from the integration of the reduction peak (the area of which was obtained by subtracting the CV of the same electrode in the absence of complex **1**, thus avoiding capacitive current), n the number of electrons in the redox process per Ni center (n = 1), F is the Faraday constant (96485 C mol^{-1}), and A is the geometrical electrode area (1 cm^2).[9]

Heterogeneous Electrochemical Studies (organic solvent)

Before controlled potential electrolysis (CPE), linear sweep voltammetry (LSV) was carried out on each sample, initially under Ar and subsequently under CO_2. Before each experiment, the solution was bubbled with gas for at least 20 minutes. Scan rate, unless otherwise stated, was 10 mVs^{-1}. A gas-tight H-shape cell with an anion exchange membrane (AMV Selemion, ACG Engineering) separating the cathode and reference electrode from the anode was used to conduct the CPE tests. The electrolyte utilized was $TBAPF_6$ 0.1 M, while the solvent was acetonitrile with 1% water content. The reference was an Ag/AgCl electrode in a saturated KCl solution, fitted with a bridge to enable operation in organic solvent, and the cathode was

a GDL on which MWCNTs and complex **1** were drop-casted as previously detailed. The anode was platinum. As an internal standard, the ferrocene/ferrocenium ($Fc^{+/}Fc^{0}$) redox couple was added at the conclusion of each measurement and used to calibrate all potentials ($E_{1/2}$ (Fc^{+}/Fc^{0}) in acetonitrile = 0.54V vs. Ag/AgCl/sat. KCl). Before beginning the electrolysis, the compartments were saturated with CO_2 for at least 20 minutes, and no additional gas was bubbled during the experiment. The experiments were conducted at room temperature and under stirring at both sides. The total volume of the cathode side of the cell was 22.6 mL, with approximately 10.6 mL of headspace volume.

The quantification of the electrolysis products (H_2, CO, and formate) followed the same procedures as in the section on homogeneous electrochemical experiments. On the basis of Equation 1, the faradaic yields were determined by quantifying the products in the head-space gas of the cathodic side (see above).

Turnover Number (TON) and Turnover Frequency (TOF) values were calculated using Equation 3 and 4, respectively:

$$TON = \frac{moles\ of\ product}{moles\ of\ catalyst} \tag{3}$$

and

$$TOF = \frac{TON}{reaction\ time\ [s]} \tag{4}$$

Heterogeneous Electrochemical Studies (water)

Before CPE, linear sweep voltammetry (LSV) was carried out on each sample, initially under Ar and subsequently under CO_2. Before each experiment, the solution was bubbled with gas for at least 20 minutes. Unless otherwise stated, 50 mV s^{-1} was the scan rate. CPE tests were conducted in a gas-tight H-shape cell with an anion exchange membrane (AMV Selemion, ACG Engineering) separating the cathode and reference electrode from the anode. The electrolyte utilized was $KHCO_3$ 0.1 M in water. The anode was platinum, the cathode was a GDL, and the reference electrode Ag/AgCl in a saturated KCl solution. MWCNTs with complex **1** were drop-cast on the working electrode as previously mentioned. Prior to each experiment, CO_2 gas was bubbled into the solution for at least 20 minutes, and a flux of CO_2 (5 mL/min) was kept during the electrolysis only on the cathode side. Experiments were carried out at room temperature.

The Nernst equation was used to convert the measured potentials vs. Ag/AgCl to the reversible hydrogen electrode (RHE) scale:

$$E_{RHE} = E_{Ag/AgCl} + 0.059\ pH + E^{o}_{Ag/AgCl} \quad (5)$$

where E_{RHE} is the converted potential vs. RHE, $E^{o}_{Ag/AgCl}$ = 0.1976 at 25 °C (sat. KCl), and $E_{Ag/AgCl}$ is the experimentally measured potential against Ag/AgCl reference and the pH of a CO_2-saturated 0.1M $KHCO_3$ solution is ~ 6.8.

The products were measured using gas chromatography (Model 8610C SRI Instruments) equipped with TCD and FID detectors to determine the faradaic yields on the basis of Equation 1 (see above).

Computational Details

DFT calculations were performed at the ωB97X-D[30] level using the Gaussian 16 (rev C01) quantum chemistry package.[31] All atoms were described by the all-electron def2-DZVP basis set.[32] Solvent effects of water were included both in geometry optimizations and energy calculations by means of the IEF-PCM implicit solvent model,[33] as implemented in Gaussian 16. Optimizations were full and without symmetry restrictions. The nature of all minima was characterized by the lack of imaginary frequencies. The Gibbs free energies of all species were corrected from the gas-phase reference state at 1 atm to the standard state of 1 mol L^{-1} in solution at 25 ºC. This corresponds to +1.9 kcal mol^{-1} for solutes and +4.3 kcal mol^{-1} for water, since acting as the solvent in this reaction, its standard state corresponds to a concentration of 55.6 mol L^{-1}. Redox potentials vs. NHE were calculated using the Nernst equation and taking an absolute potential of 4.42 V for NHE.[34] Then, these were translated into the RHE scale by applying a + 0.059 × pH shift, using a pH value of 6.8.

Periodic DFT calculations to evaluate the possible impact of the catalyst-support interaction on the electronic structure of the catalyst were performed with the Vienna ab initio simulation package (VASP) 5.3.3,[35–38] to optimize geometries and calculate electronic energies at 0 K in vacuum. Plane-wave basis sets via the projector augmented wave method (PAW)[39,40] were used to describe the wave function close to the nuclei. The wave function was expanded, in terms of plane-wave basis sets with a cut-off energy of 500 eV. Exchange and correlation energies were calculated using the Perdew-Burke-Ernzerhof functional (PBE).[41] Due to the presence of van der Waals (vdW) interactions inherent to carbon ring structures, the DFT-D3 correction method of Grimme et al.[42] was applied. The partial occupancies close to the Fermi level were described by the first-order Methfessel Paxton method which was applied with a smearing width of 0.1 eV. The electronic energy convergence was set to 1×10^{-6} eV.

The geometry optimization was carried out until the maximum forces on the atoms were lower than 1×10^{-2} eV $Å^{-1}$ using the Davidson and RMM-DIIS algorithms.[43] These convergence criteria were set as reported on previous studies on graphene based materials.[44] The catalysts were simulated by repeating the unit cell in three directions to create a periodic surface slab model. Brillouin-zone integration was sampled with a Monkhorst-Pack mesh with a 5×5×1 grid in reciprocal space in the case of the surface calculations.[45] For all calculations a vacuum layer of 20 Å was included in the axial direction, coupled with an artificial dipole layer to avoid interactions between periodic images.[46]

Acknowledgements

S.P. acknowledges financial support from the European School on Artificial Leaf: Electrodes & Devices (eSCALED). This project has received funding from the European's Union's Horizon 2020 research and innovation programme under the Marie Sklodowska-Curie grant agreement No 765376.

Supporting Information

Crystallographic data for complex **1**, Homogeneous and heterogeneous electrochemical Studies for complex **1**, additional electrodes characterization, Theoretical DFT calculations (DOC)

References

[1] L. Rotundo, R. Gobetto, C. Nervi. Electrochemical CO_2 reduction with earth-abundant metal catalysts. *Curr. Opin. Green Sustain. Chem.*, **2021**, *31*, 100509.

[2] C. Sun, R. Gobetto, C. Nervi. Recent advances in catalytic CO_2 reduction by organometal complexes anchored on modified electrodes. *New J. Chem.*, **2016**, *40*, 5656–5661.

[3] N. Elgrishi, M. B. Chambers, X. Wang, M. Fontecave. Molecular polypyridine-based metal complexes as catalysts for the reduction of CO_2. *Chem. Soc. Rev.*, **2017**, *46*, 761–796.

[4] L. Sun, V. Reddu, A. C. Fisher, X. Wang. Electrocatalytic reduction of carbon dioxide: Opportunities with heterogeneous molecular catalysts. *Energy Environ. Sci.*, **2020**, *13*, 374–403.

[5] Y. Wu, Z. Jiang, X. Lu, Y. Liang, H. Wang. Domino electroreduction of CO_2 to methanol on a molecular catalyst. *Nature*, **2019**, *575*, 639–642.

[6] X. Zhang, Y. Wang, M. Gu, M. Wang, Z. Zhang, W. Pan, Z. Jiang, H. Zheng, M. Lucero, H. Wang, G. E. Sterbinsky, Q. Ma, Y. G. Wang, Z. Feng, J. Li, H. Dai, Y. Liang. Molecular engineering of dispersed nickel phthalocyanines on carbon nanotubes for selective CO_2 reduction. *Nat. Energy*, **2020**, *5*, 684–692.

[7] X. M. Hu, S. U. Pedersen, K. Daasbjerg. Supported molecular catalysts for the heterogeneous CO_2 electroreduction. *Curr. Opin. Electrochem.*, **2019**, *15*, 148–154.

[8] J. D. Blakemore, A. Gupta, J. J. Warren, B. S. Brunschwig, H. B. Gray. Noncovalent immobilization of electrocatalysts on carbon electrodes for fuel production. *J. Am. Chem. Soc.*, **2013**, *135*, 18288–18291.

[9] B. Reuillard, K. H. Ly, T. E. Rosser, M. F. Kuehnel, I. Zebger, E. Reisner. Tuning Product Selectivity for Aqueous CO_2 Reduction with a Mn(bipyridine)-pyrene Catalyst Immobilized on a Carbon Nanotube Electrode. **2017**, DOI 10.1021/jacs.7b06269.

[10] M. Beley, J. P. Collin, R. Ruppert, J. P. Sauvage. Nickel(II)-Cyclam: An Extremely Selective Electrocatalyst for Reduction of CO_2 in Water. *J. Chem. Soc. - Ser. Chem. Commun.*, **1984**, *2*, 1315–1316.

[11] A. Zhanaidarova, C. E. Moore, M. Gembicky, C. P. Kubiak. Covalent attachment of [Ni(alkynyl-cyclam)]$^{2+}$ catalysts to glassy carbon electrodes. *Chem. Commun.*, **2018**, *54*, 4116–4119.

[12] S. Pugliese, N. T. Huan, J. Forte, D. Grammatico, S. Zanna, B. L. Su, Y. Li, M. Fontecave. Functionalization of Carbon Nanotubes with Nickel Cyclam for the Electrochemical Reduction of CO_2. *ChemSusChem*, **2020**, *13*, 6449–6456.

[13] Y. Wu, B. Rudshteyn, A. Zhanaidarova, J. D. Froehlich, W. Ding, C. P. Kubiak, V. S. Batista. Electrode-Ligand Interactions Dramatically Enhance CO_2 Conversion to CO by the [Ni(cyclam)]$(PF_6)_2$ Catalyst. *ACS Catal.*, **2017**, *7*, 5282–5288.

[14] F. Greenwell, G. Neri, V. Piercy, A. J. Cowan. Noncovalent immobilization of a nickel cyclam catalyst on carbon electrodes for CO_2 reduction using aqueous electrolyte. *Electrochim. Acta*, **2021**, *392*, 139015.

[15] C. C. Liolios, C. Zikos, E. Fragogeorgi, D. Benaki, M. Pelecanou, I. Pirmettis, N. Ioannidis, Y. Sanakis, C. P. Raptopoulou, V. Psycharis, A. Terzis, F. Boschetti, M. S. Papadopoulos, G. Sivolapenko, A. D. Varvarigou. A Bombesin Copper Complex Based on a Bifunctional Cyclam Derivative. *Eur. J. Inorg. Chem.*, **2012**, *2012*, 2877–2888.

[16] B. Bosnich, R. Mason, P. J. Pauling, G. B. Robertson, M. L. Tobe. The molecular structure of dichloro-1,4,8,11-tetra-azacyclotetradecanenickel(II). *Chem. Commun.*, **1965**, *346*, 97.

[17] J. Song, E. L. Klein, F. Neese, S. Ye. The Mechanism of Homogeneous CO_2 Reduction by Ni(cyclam): Product Selectivity, Concerted Proton–Electron Transfer and C–O Bond Cleavage. *Inorg. Chem.*, **2014**, *53*, 7500–7507.

[18] C. Costentin, M. Robert, J.-M. Savéant. Catalysis of the electrochemical reduction of carbon dioxide. *Chem. Soc. Rev.* **2013**, *42*, 2423**–**2436.

[19] M. Wang, K. Torbensen, D. Salvatore, S. Ren, D. Joulié, F. Dumoulin, D. Mendoza, B. Lassalle-Kaiser, U. Işci, C. P. Berlinguette, M. Robert. CO_2 electrochemical catalytic reduction with a highly active cobalt phthalocyanine. *Nat. Commun.*, **2019**, *10*.

[20] J. D. Froehlich, C. P. Kubiak. The Homogeneous Reduction of CO_2 by [Ni(cyclam)]$^+$: Increased Catalytic Rates with the Addition of a CO Scavenger. *J. Am. Chem. Soc.*, **2015**, *137*, 3565–3573.

[21] C. Jiang, A. W. Nichols, J. F. Walzer, C. W. MacHan. Electrochemical CO_2 Reduction in a Continuous Non-Aqueous Flow Cell with $[Ni(cyclam)]^{2+}$. *Inorg. Chem.*, **2020**, 59, 3, 1883–1892.

[22] S. L. Behnke, A. C. Manesis, H. S. Shafaat. Spectroelectrochemical investigations of nickel cyclam indicate different reaction mechanisms for electrocatalytic CO_2 and H^+ reduction. *Dalt. Trans.*, **2018**, *47*, 15206–15216.

[23] C. A. Kelly, Q. G. Mulazzani, M. Venturi, E. L. Blinn, M. A. J. Rodgers. The Thermodynamics and Kinetics of CO_2 and H^+ binding to $Ni(cyclam)^+$ in Aqueous Solution. *J. Am. Chem. Soc.*, **1995**, *117*, 4911–4919.

[24] M. Zhu, J. Chen, L. Huang, R. Ye, J. Xu, Y. Han. Covalently Grafting Cobalt Porphyrin onto Carbon Nanotubes for Efficient CO_2 Electroreduction. *Angew. Chemie*, **2019**, *131*, 6667–6671.

[25] M. Wang, L. Chen, T.-C. Lau, M. Robert. A Hybrid Co Quaterpyridine Complex/Carbon Nanotube Catalytic Material for CO_2 Reduction in Water. *Angew. Chemie*, **2018**, *130*, 7895–7899.

[26] T. D. Cook, S. F. Tyler, C. M. McGuire, M. Zeller, P. E. Fanwick, D. H. Evans, D. G. Peters, T. Ren. Nickel Complexes of C-Substituted Cyclams and Their Activity for CO_2 and H^+ Reduction. *ACS Omega*, **2017**, *2*, 3966–3976.

[27] B. Siritanaratkul, M. Forster, F. Greenwell, P. K. Sharma, E. H. Yu, A. J. Cowan. Zero-Gap Bipolar Membrane Electrolyzer for Carbon Dioxide Reduction Using Acid-Tolerant Molecular Electrocatalysts. *J. Am. Chem. Soc.*, **2022**, 144, 17, 7551–7556.

[28] D. C. Miller, G. J. Choi, H. S. Orbe, R. R. Knowles. Catalytic Olefin Hydroamidation Enabled by Proton-Coupled Electron Transfer. *J. Am. Chem. Soc.*, **2015**, *137*, 13492–13495.

[29] S. J. Krivickas, E. Tamanini, M. H. Todd, M. Watkinson. Effective methods for the biotinylation of azamacrocycles. *J. Org. Chem.*, **2007**, *72*, 8280–8289.

[30] J.-D. Chai, M. Head-Gordon. Long-range corrected hybrid density functionals with damped atom–atom dispersion corrections. *Phys. Chem. Chem. Phys.*, **2008**, *10*, 6615–6620.

[31] M. J. Frisch, G. W. Trucks, H. B. Schlegel, G. E. Scuseria, M. a. Robb, J. R. Cheeseman, G. Scalmani, V. Barone, G. a. Petersson, H. Nakatsuji, X. Li, M. Caricato,

a. V. Marenich, J. Bloino, B. G. Janesko, R. Gomperts, B. Mennucci, H. P. Hratchian, J. V. Ortiz, a. F. Izmaylov, J. L. Sonnenberg, Williams, F. Ding, F. Lipparini, F. Egidi, J. Goings, B. Peng, A. Petrone, T. Henderson, D. Ranasinghe, V. G. Zakrzewski, J. Gao, N. Rega, G. Zheng, W. Liang, M. Hada, M. Ehara, K. Toyota, R. Fukuda, J. Hasegawa, M. Ishida, T. Nakajima, Y. Honda, O. Kitao, H. Nakai, T. Vreven, K. Throssell, J. a. Montgomery Jr., J. E. Peralta, F. Ogliaro, M. J. Bearpark, J. J. Heyd, E. N. Brothers, K. N. Kudin, V. N. Staroverov, T. a. Keith, R. Kobayashi, J. Normand, K. Raghavachari, a. P. Rendell, J. C. Burant, S. S. Iyengar, J. Tomasi, M. Cossi, J. M. Millam, M. Klene, C. Adamo, R. Cammi, J. W. Ochterski, R. L. Martin, K. Morokuma, O. Farkas, J. B. Foresman, D. J. Fox. G16_C01. **2016**, Gaussian 16, Revision C.01, Gaussian, Inc., Wallin.

[32] F. Weigend, R. Ahlrichs. Balanced basis sets of split valence, triple zeta valence and quadruple zeta valence quality for H to Rn: Design and assessment of accuracy. *Phys. Chem. Chem. Phys.*, **2005**, *7*, 3297.

[33] E. Cancès, B. Mennucci, J. Tomasi. A new integral equation formalism for the polarizable continuum model: Theoretical background and applications to isotropic and anisotropic dielectrics. *J. Chem. Phys.*, **1997**, *107*, 3032–3041.

[34] M. D. Tissandier, K. A. Cowen, W. Y. Feng, E. Gundlach, M. H. Cohen, A. D. Earhart, J. V Coe, T. R. Tuttle. The Proton's Absolute Aqueous Enthalpy and Gibbs Free Energy of Solvation from Cluster-Ion Solvation Data. *J. Phys. Chem. A*, **1998**, *102*, 7787–7794.

[35] G. Kresse, J. Hafner. Ab initio molecular-dynamics simulation of the liquid-metal–amorphous-semiconductor transition in germanium. *Phys. Rev. B*, **1994**, *49*, 14251–14269.

[36] G. Kresse, J. Hafner. Ab initio molecular dynamics for liquid metals. *Phys. Rev. B*, **1993**, *47*, 558–561.

[37] G. Kresse, J. Furthmüller. Efficient iterative schemes for ab initio total-energy calculations using a plane-wave basis set. *Phys. Rev. B*, **1996**, *54*, 11169–11186.

[38] G. Kresse, J. Furthmüller. Efficiency of ab-initio total energy calculations for metals and semiconductors using a plane-wave basis set. *Comput. Mater. Sci.*, **1996**, *6*, 15–50.

[39] P. E. Blöchl. Projector augmented-wave method. *Phys. Rev. B*, **1994**, *50*, 17953–17979.

[40] G. Kresse, D. Joubert. From ultrasoft pseudopotentials to the projector augmented-wave method. *Phys. Rev. B*, **1999**, *59*, 1758–1775.

[41] J. P. Perdew, K. Burke, M. Ernzerhof. Generalized Gradient Approximation Made Simple. *Phys. Rev. Lett.*, **1996**, *77*, 3865–3868.

[42] S. Grimme, J. Antony, S. Ehrlich, H. Krieg. A consistent and accurate ab initio parametrization of density functional dispersion correction (DFT-D) for the 94 elements H-Pu. *J. Chem. Phys.*, **2010**, *132*, 154104.

[43] P. Pulay. Convergence acceleration of iterative sequences. the case of scf iteration. *Chem. Phys. Lett.*, **1980**, *73*, 393–398.

[44] J. Zhao, J. Zhao, F. Li, Z. Chen. Copper dimer supported on a C_2N layer as an efficient electrocatalyst for CO_2 reduction reaction: A computational study. *J. Phys. Chem. C*, **2018**, *122*, 19712–19721.

[45] D. J. Chadi, M. L. Cohen. Special Points in the Brillouin Zone. *Phys. Rev. B*, **1973**, *8*, 5747–5753.

[46] G. Makov, M. C. Payne. Periodic boundary conditions in ab initio calculations. *Phys. Rev. B*, **1995**, *51*, 4014–4022.

For Table of Contents Only

TOC graphic

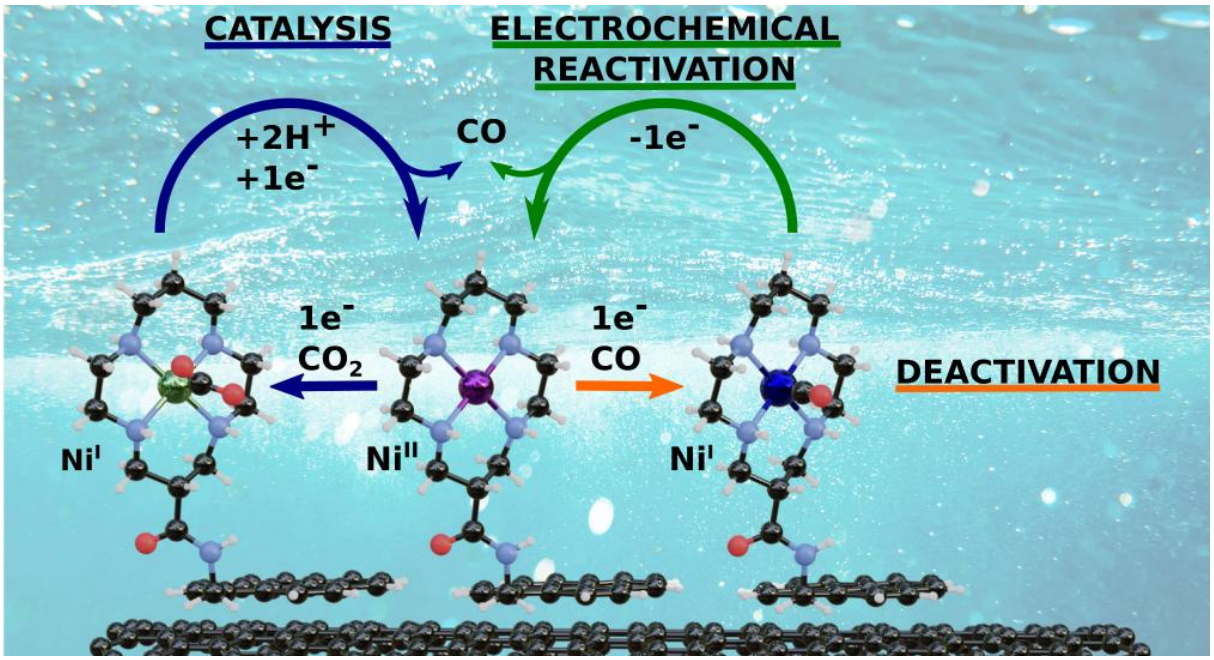

Synopsis

We report a novel $[Ni(cyclam)]^{2+}$ complex which can be immobilized on carbon nanotubes. Deposited on a gas diffusion layer, it provides an electrode selective for CO_2 electroreduction to CO, not only in organic solvents but, more remarkably, in water, with faradic efficiencies for CO > 85 % and current densities of 5-10 $mA.cm^{-2}$ during electrolysis. Inactivation occurs in water due to the formation of a Ni-CO complex. However, the electrode can be electrochemically reactivated.